JACS
JOURNAL OF THE AMERICAN CHEMICAL SOCIETY
Article
pubs.acs.org/JACS

Insight into Proton Transfer in Phosphotungstic Acid Functionalized Mesoporous Silica-Based Proton Exchange Membrane Fuel Cells

Yuhua Zhou,[†] Jing Yang,[†] Haibin Su,*[,†,‡] Jie Zeng,[§] San Ping Jiang,*[,§] and William A. Goddard*[,∥]

[†]School of Materials Science and Engineering, Nanyang Technological University, 50 Nanyang Avenue, 639798 Singapore

[‡]Institute of High Performance Computing, 1 Fusionopolis Way, Connexis 138632, Singapore

[§]Fuels and Energy Technology Institute & Department of Chemical Engineering, Curtin University, Perth, Western Australia 6102, Australia

[∥]Materials and Process Simulation Center, California Institute of Technology, Pasadena, California 91125, United States

Supporting Information

ABSTRACT: We have developed for fuel cells a novel proton exchange membrane (PEM) using inorganic phosphotungstic acid (HPW) as proton carrier and mesoporous silica as matrix (HPW-*meso*-silica) . The proton conductivity measured by electrochemical impedance spectroscopy is 0.11 S cm^{-1} at 90 °C and 100% relative humidity (RH) with a low activation energy of ~14 kJ mol^{-1}. In order to determine the energetics associated with proton migration within the HPW-*meso*-silica PEM and to determine the mechanism of proton hopping, we report density functional theory (DFT) calculations using the generalized gradient approximation (GGA). These DFT calculations revealed that the proton transfer process involves both intramolecular and intermolecular proton transfer pathways. When the adjacent HPWs are close (less than 17.0 Å apart), the calculated activation energy for intramolecular proton transfer within a HPW molecule is higher (29.1−18.8 kJ/mol) than the barrier for intermolecular proton transfer along the hydrogen bond. We find that the overall barrier for proton movement within the HPW-*meso*-silica membranes is determined by the intramolecular proton transfer pathway, which explains why the proton conductivity remains unchanged when the weight percentage of HPW on *meso*-silica is above 67 wt %. In contrast, the activation energy of proton transfer on a clean SiO_2 (111) surface is computed to be as high as ~40 kJ mol^{-1}, confirming the very low proton conductivity on clean silica surfaces observed experimentally.

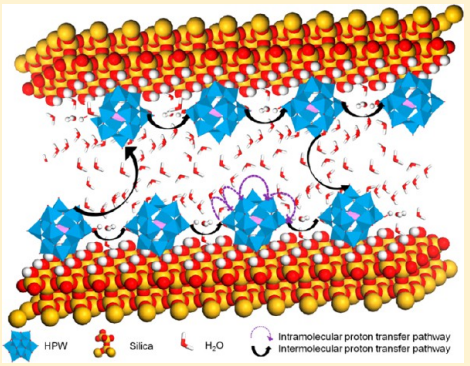

1. INTRODUCTION

Proton exchange membrane fuel cells (PEMFCs) have attracted great attention because of their high power density and high efficiency combined with low greenhouse gas emission, which is highly desirable for a broad range of applications in clean energy technologies, electric vehicles, portable electronics, and domestic power generation.[1−5] PEMFCs based on state-of-the-art perfluorosulfonic acid (PFSA) membranes, such as Nafion, generally must operate at low temperatures (≤80 °C). This is because the proton conductivity of Nafion membranes deteriorates rapidly at elevated temperature (>85 C) because of the loss of water, leading to the significant loss in cell performance. However, low temperature operations lead to two difficulties: (1) low temperature PEM fuel cells are prone to poisoning by impurities in fuels such as carbon monoxide and (2) because of the nature of the Nafion-based membrane, a rather complicated water management system must be implemented to prevent the flooding/drying of the membrane-electrode-assembly system. Therefore, developing novel PEMs with both structural stability and high proton conductivity at elevated temperature is of critical significance for attaining the required PEMFC performance.

Consequently intensive efforts have been made to generate alternative proton conductive materials for operation at elevated temperatures. Among these is the formation of composite membranes with such inorganic materials,[6] as heteropoly acids (HPAs). The HPAs have the highest known proton conductivities and offer an excellent opportunity for creating a material with heretofore unachieved combinations of both low-temperature and high-temperature performance.[7] However, HPAs are water-soluble and must be immobilized and appropriately organized to form practical materials with high proton conductivities. Despite their conductivity as low as 10^{-6} to 10^{-4} S cm^{-1}, mesoporous silica materials hold great potential as porous frameworks for high temperature PEM applications. This is because of the remarkable structural order, large surface areas and pore volumes, and the readily variable surface functionalization.[8] Through such functionalization methods as grafting sulfonic side groups onto the external

Received: November 14, 2013
Published: March 14, 2014

   dx.doi.org/10.1021/ja411268q | J. Am. Chem. Soc. 2014, 136, 4954−4964

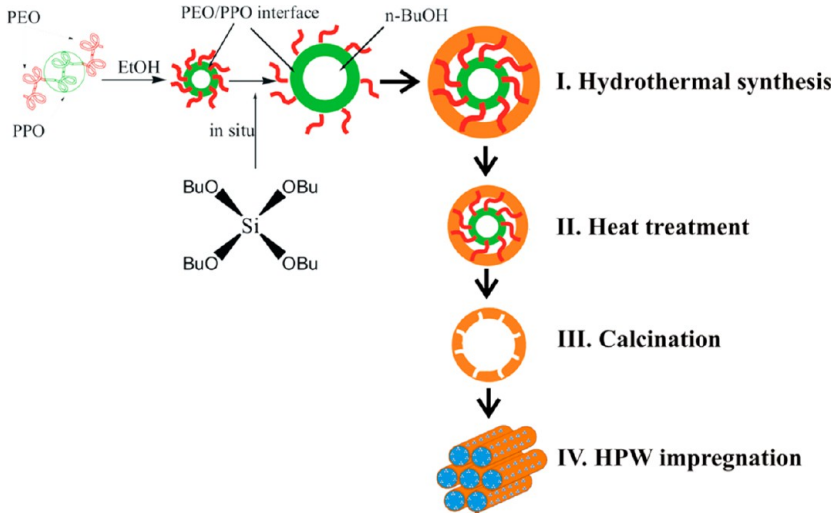

Figure 1. Procedure of the synthesis processes for mesoporous silica and HPW-*meso*-silica composite.

Si−O site,[9] the synthesized *meso*-SiO_2−$C_{12}EO_{10}OH$−CF_3SO_3H materials provide promising new proton conducting electrolyte with a conductivity of 1×10^{-3} S cm^{-1} at room temperature and 90% RH (relative humidity).[10] Incorporating various HPAs into silicaphosphate porous glass, Nogami et al.[11] obtained electrolyte membranes with high proton conductivity. As examples, the $H_3PW_{12}O_{40}$ (HPW) and $H_3PMo_{12}O_{40}$ (HPM) inorganic glass composite membrane was reported to have a conductivity of 1.014 S cm^{-1} at 30 °C and 85% RH, while the mesoporous HPW/HPM-P_2O_5−SiO_2 glass[12] has a conductivity of 1.01×10^{-1} S cm^{-1} at 85 °C and 85% RH.[13]

On the basis of using highly ordered mesoporous silica, we recently developed a new inorganic HPW-impregnated mesoporous silica (HPW-*meso*-silica) nanocomposite proton exchange membrane.[14] Our best results were obtained with body-centered cubic HPW-*meso*-silica membranes, which achieved a proton conductivity of 0.061 S cm^{-1} at 25 °C and 0.14 S cm^{-1} at 150 °C. Most significantly, in contrast to conventional Nafion membranes, the proton conductivity of HPW-*meso*-silica membranes shows high tolerance to RH fluctuations. For example, under 80% RH, the power density of the cell with HPW-*meso*-silica membrane is 308 mW cm^{-2} in H_2/O_2, and it is 215 mW cm^{-2} as the RH decreases to 20%. The decrease in power density is 30%, which is 3 times smaller than that of the cell with Nafion 115 membranes under identical test conditions.[14b] This indicates the excellent water retention capability of the HPW-*meso*-silica nanocomposites. The cells based on the HPW-*meso*-silica membrane achieved a maximum power density of 237 mW cm^{-2} in methanol fuel at 150 °C with no external humidification. HPW-*meso*-silica membranes can also be synthesized via an efficient, one-step self-assembly route assisted by structure-directing surfactants.[15] This self-assembled HPW-*meso*-silica exhibited a high proton conductivity of 0.091 S cm^{-1} at 100 °C with a low activation energy ~13.0 kJ mol^{-1}, achieving a maximum power density of 19 mW cm^{-2} at room temperature and 235 mW cm^{-2} at 150 °C in methanol fuel on cells with a 200 μm thick 25 wt % HPW-*meso*-silica membrane. These experimental results demonstrate the promising potential of HPW-*meso*-silica as an alternative PEMs for operation at elevated temperatures and reduced RH conditions.

Our newly developed HPW-*meso*-silica composite membranes have been characterized extensively, including transmission electron microscopy (TEM) and small-angle X-ray scattering (SAXS), providing direct observations relevant to the morphology and distribution of HPW nanoparticles in mesoporous channels, TGA (thermogravimetric analysis) for detecting the thermal stability of HPW and water uptake of the composite membrane. In addition electrochemical impedance spectroscopy to measure the high proton conductivity at various temperatures and RH has been used to determine the low activation energy through Arrhenius plots. However, the mechanisms of proton migration within HPW-*meso*-silica electrolyte remain largely unknown. The fundamental understanding of the mechanisms for proton migration and transfer in the HPW-functionalized mesoporous silica channels and how this affects the activation barrier for proton conductivity is critical for further development and optimization of the heteropolyacid-based PEMs for fuel cells and solid acid catalysis. Thus we carried out quantum chemical calculations to provide this understanding of how the nature of self-assembled HPW-*meso*-silia affects proton conductivity. Previous density functional theory (DFT) studies[16] of the motion of protons *within* an isolated single Keggin unit (KU) HPW described the dependence of the proton-hopping rate on the humidity. They demonstrated that the adsorption of water substantially reduces the energy barrier of proton hopping from 117.9 to 19.1 kJ mol^{-1}.

In this work, we consider a novel inorganic PEM based on highly ordered mesoporous silica with assembled HPW nanoparticles and use electrochemical impedance spectroscopy to determine the proton conductivity as a function of temperature to obtain the experimental activation energy as a function of the weight ratio of HPW (wt %). We also carry out DFT calculations at the generalized gradient approximation (GGA) level to evaluate the mechanism of proton migration within the HPW-*meso*-silica electrolyte. In particular we determine the movement of protons *between* two nearest KU HPWs, which we compare to the proton hopping *within* a single KU. Combining the results from these theoretical and experimental studies, we address the critical and substantial factors controlling the proton conductivity within the HPW-*meso*-silica PEM to provide guidance on further optimization of the design and operation of HPW-*meso*-silica-based PEMs for fuel cells.

dx.doi.org/10.1021/ja411268q | J. Am. Chem. Soc. 2014, 136, 4954−4964

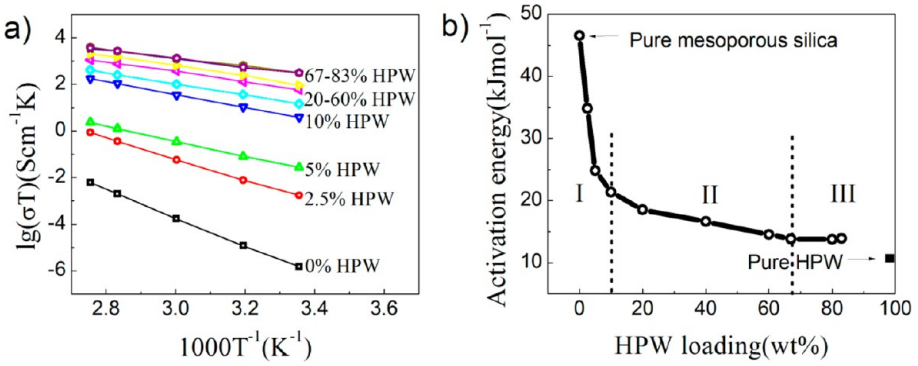

Figure 2. (a) Proton conductivity versus temperature of the HPW-*meso*-silica composite membranes as a function of HPW loading, and (b) activation energy versus HPW content of HPW-*meso*-silica membrane measured at 25 °C.

2. EXPERIMENTAL STUDIES

Ordered mesoporous silica with the cubic bicontinuous structure ($Ia\bar{3}d$) was prepared according to the synthesis method reported by Zhao and his co-workers.[17] As depicted in Figure 1,[18] bicontinuous cubic $Ia\bar{3}d$ mesoporous silica was prepared by using triblock copolymer P123 ($EO_{20}PO_{70}EO_{20}$, Sigma-Aldrich) as a template under acid condition. The anionic surfactant sodium dodecylbenzene sulfonate (SDBS, Sigma-Aldrich) was used as an additive to induce the self-assembly. Typically 2.3 g of SDBS (6 mM) was first dissolved in a solution containing 20 g of triblock copolymer P123, 32 g of HCl (67%), and 720 g of deionized water (18.2 MΩ), and stirred until a homogeneous solution formed. Then 43 g of tetraethyl orthosilicate (TEOS, Sigma-Aldrich) was added to the solution, the mixture was further stirred at 45 °C for 24 h, and then it was transferred into a hydrothermal reactor for hydrothermal treatment at 100 °C for another 24 h. The product was filtered and washed thoroughly with water and then air-dried overnight. The as-synthesized powder was calcined at 650 °C in air for 6 h to remove the block copolymer template. The calcinations process started from room temperature with a ramping rate of 1 °C min^{-1}, and N_2 was used as protective atmosphere at temperatures below 200 °C. The mesoporous silica was functionalized with HPW by impregnation of the mesoporous silica in HPW aqueous solution (400 g of HPW in 100 mL of water) under a vacuum at room temperature for 8 h. The powder was collected after drying at 80 °C overnight. For the conductivity measurements the HPW-*meso*-silica membrane was prepared by hot-pressing at 180 °C for 2 h. The disc samples have a diameter of 3.8 cm and thickness of around 500 μm. The proton conductivity measurements of HPW-*meso*-silica were performed using a four-probe method in conjunction with electrochemical impedance spectroscopy (PGSTAT30/FRA, Autolab. Netherlands) over the frequency range from 1 Hz to 1 MHz in the temperatures range from 20 to 90 °C under 100% RH. The HPW concentration impregnated in *meso*-silica matrix varied between 0 and 83%. The relative humidity of the proton conductivity measurements was controlled by a commercial PEMFC test station (FCATS-G050, Greenlight, Canada).

The stability of the proton conductivity of HPW-*meso*-silica was investigated under an accelerated durability test.[14a,18] In this test, the conductivity was measured in a single cell with continuous flow of deionized water on both sides of the membrane. For example, in the case of vacuum assisted impregnated 30% HPW-*meso*-silica nanocomposite membrane, the initial conductivity is 0.023 S cm^{-1} and stabilized at 0.014 S cm^{-1} after testing under continuous water flow at 50 °C. In contrast, the conductivity of a simply mixed HPW-mesoporous silica membrane reaches zero after 10 h under the same testing conditions.[14a] This indicates that impregnated HPW is quite stable inside the mesopores of the mesoporous silica matrix structure. Similar proton conductivity stability was also observed on the self-assembled HPW-*meso*-silica nanocomposites.[15c] The high stability of proton conductivity of HPW-*meso*-silica nanocomposites under accelerated durability test indicates that HPW must be *anchored* rather than simply physically adsorbed on the external siliceous walls of mesoporous silica. This is exactly the case as shown by ^{31}P MAS NMR studies.[15b] In this study, the hydrated HPW displays one main peak at −15.6 ppm, indicating that the Keggin units are coordinated to their neighboring units by H_3O^+.[19] After the assembly of HPW inside the mesoporous silica, a single peak is observed at −15.0 ppm in the ^{31}P MAS NMR spectrum.[15b] Such a chemical shift of the ^{31}P MAS NMR peak has been attributed to the strong chemical interactions between HPW and silica surface, as indicated by Lefebvre.[20]

Figure 2a shows the conductivity (σ) of HPW-*meso*-silica nanocomposites measured at various temperatures as a function of HPW content.[14b] We find that the proton conductivity is as low as 1.4×10^{-5} S cm^{-1} for pure *meso*-silica but increases significantly after the functionalization by HPW. The proton conductivity depends strongly on the HPW content. With impregnation of small amounts of HPW (e.g., 2.5 to 5 wt % HPW), the proton conductivity of *meso*-silica increases remarkably (4.5×10^{-2} S cm^{-1} for 5 wt % HPW-*meso*-silica). However for an HPW content above 10 wt %, there is little further increase in the proton conductivity. Above a HPW content of 67 wt %, the conductivity of HPW-*meso*-silica was almost independent of the HPW. Thus this study indicates that the maximum conductivity of the HPW-*meso*-silica nanocomposites is ∼0.11 S cm^{-1} at 25 °C, which is close to 0.18 S cm^{-1} of fully hydrated HPW.[21]

The activation energy (E_a) was calculated by linear regression of the Arrhenius plots with σ and ln T. It is characterized by three distinct regions as shown in Figure 2b, which depend on the weight percentage of HPW:

(1) The highest energy activation barrier of about 46.0 kJ mol^{-1} is found for 0 wt % HPW anchoring on *meso*-silica surface of $Ia\bar{3}d$ structure, which is very close to the results reported in the literature.[8a]

(2) With a small amount of HPW adsorbing on silica surface (2.5−10 wt % HPW), the energy barrier decreased significantly to ∼20 kJ mol^{-1}.

(3) Continuing to increase the content of HPW in the range of 20−60 wt %, the energy barrier decreases modestly with HPW. The final activation energy, E_a is only around 14.0 kJ mol^{-1} for HPW contents of 67 wt % or above. This high proton conductivity and low activation energy for HPW content in the *meso*-silica above the threshold value of ∼10 wt % indicates the establishment of effective proton transfer pathways within the HPW-*meso*-silica nanocomposite.

3. COMPUTATIONAL METHODS

All DFT computations were carried out using the generalized gradient approximation (GGA) functional of Perdew, Burke, and Ernzerhof (PBE).[22,23] In these calculations we described all electrons explicitly (no pseudopotential) for both the H, O, P and Si elements and W (where we also included relativistic effects into the core).[24] The basis set included polarization functions. We used the fine quality mesh size for the numerical integration. We used a real space cutoff for the atomic basis functions of 4.6 Å, which was chosen to increase computational efficiency while not significantly affecting the magnitude of interatomic forces or the total energies. The self-consistent-field calculation used a convergence criteria of 1×10^{-6} e/

dx.doi.org/10.1021/ja411268q | J. Am. Chem. Soc. 2014, 136, 4954−4964

Å. The tolerances of energy, gradient, and the displacement for the geometry optimization were set to be 2×10^{-5} au, 4×10^{-4} Å, and 5×10^{-4} Å, respectively.

To investigate the proton transport in mesoporous silica, we chose the most stable surface of silica, i.e., the ideal (111) surface of β cristobalite.[25] We described the periodic SiO_2(111) surface using both 2×2 and 3×3 unit cells and considered a slab thickness of four layers with the top two layers fully relaxed during geometry optimization. A $2 \times 2 \times 1$ k-point grid was used to describe the first Brillouin zone. We used a vacuum region of 15 Å thickness to separate the surface from its periodic image in the direction normal to the surface. Because of extreme difficulty in converging periodic SiO_2 slab models, we used a thermal smearing value of 0.02 hartree to facilitate the optimization process.

To describe the minimum energy pathway for proton-hopping reactions, we used the combined linear synchronous transition/quadratic synchronous transit (LST/QST)[26] method to locate the transition state (TS), which has been well validated for finding the structure at the transition state and the minimum energy pathway.

4. RESULTS AND DISCUSSIONS

$H_3PW_{12}O_{40}$ is a well-known member of the HPAs class having the strongest acidity.[27,28] The most common structure is KU as shown in Figure 3, which is the basic unit for constructing the

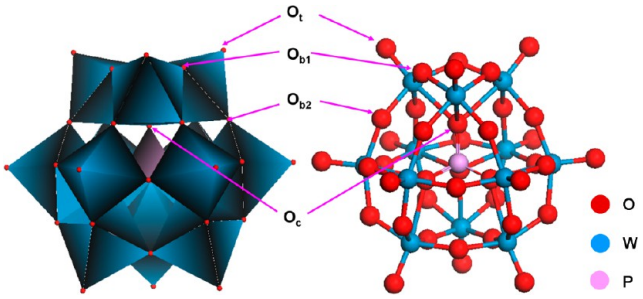

Figure 3. The Keggin structure of anion phosphotungstic acid ($PW_{12}O_{40}^{3-}$): O_t, O_{b1}, O_{b2}, and O_c labled the four types of oxygen in the structure (oxygen atoms in red; tungsten in cyan; phosphor in magenta).

primary structure of the HPAs leading to the best acid strength, stability, and availability compared to other polyoxometalates. The central phosphorus (P) atom is in a tetrahedral environment surrounded by 12 octahedral of composition WO_6. The oxygen atoms are all shared between tungsten atoms, except for 12 terminal oxygen atoms (O_t) attached to only one W atom. Normally, protons coordinate to oxygen atoms on the exterior of the KU to obtain the primary structure of the heteropoly acid. Then adsorbed water molecules interact with oxygen atoms of adjacent KUs via hydrogen bonds, linking the units together to form a secondary structure. The effect of water on proton conductivity of HPW is most pertinent to the properties of HPW in the PEM fuel cells.

Under normal pH range or neutral solutions, the proton adsorption on SiOH surface group of the mesoporous silica walls is very low and siliceous walls are typically neutral. However, HPW has the strongest acidity among the Keggin-type heteropolyacids. The presence of highly acidic HPW significantly increases the positive charge accumulated on silica surface,[29] leading to the rapid increase in zeta potential and the formation of positively charged functional groups. The HPW Keggin unit contains three negative charges, which are neutralized in the acid solution by protons in the form of acidic hydroxyl groups. Within the HPW-*meso*-silica membrane, the negatively charged heteropolyacid $PW_{12}O_{40}^{3-}$ units anchored by self-assembly onto the positively charged silica channels through electrostatic interactions. Our TEM results[14] provide direct observation of the morphology and distribution of HPW nanoparticles in the highly ordered mesoporous silica channels. This is due to the phase contrast between HPW and silica (tungsten atoms of HPW are much heavier than silicon atoms of silica), with the distances between HPW varying according to the weight percentage of HPW. For example, in the case of 20% HPW-*meso*-silica nanocomposites, the distances between the HPW particles in the mesopores vary between 1 to 10 nm.[14b] The case of 80 wt % HPW-*meso*-silica nanocomposites shows the shortest distance between neighbor HPW molecules of around 1.0 to 1.5 nm.[18] Here, the energy barrier for proton migration is lowest, making the conductivity highest. As the weight percentage decreases, the average distance between HPWs increases, leading to the increase in the energy barrier for proton transfer, and concomitantly a decrease of conductivity (see Figure 2). Obviously, the average distances between HPWs, determined by the weight percentage of HPW, affect both the proton conductivity and energy barrier of proton transfer.

Figure 4 shows the scheme of the ordered mesoporous arrays with anchored HPW inside the walls of the nanochannels of the mesoporous silica, which depicts the effective proton transport pathways in the mesoporous channels. This figure shows two effective pathways determining the rate of proton transfer. One is the intramolecular proton transfer pathway, in which the proton-hopping happens on an isolated HPW. The other is the intermolecular proton transfer pathway, involving a series of "hops" from one HPW to the neighboring HPW along the water-assisted hydrogen bond. Obviously, the rate-limited step is the pathway having the highest energy barrier, which determines the overall proton conductivity of self-assembled HPW-*meso*-silica.

4.1. IntraHPW Proton Hopping. From the structure of KU shown in Figure 3, there are three types of oxygen atoms available for the proton. We used DFT calculations to predict the proton affinity for the proton at various oxygen sites on the exterior of the molecular HPW, which provided the relative acid strength. Our results suggest that the proton prefers two types of bridging oxygen atoms (O_b) compared to the terminal oxygen atoms (O_t) by 54.03 to 61.75 kJ mol^{-1} (see Supporting Information).

First we studied the intramolecular pathway, which considers only the proton movement within an isolated HPW molecule. Here, we considered only the one jump path between the O_{b1} and O_t atoms to determine the proton-transfer reaction within a single KU HPW molecule. In addition, in order to check the effect of water on the energy barrier of intramolecular proton transfer, we compared the pathway assisted with one or two water molecules with that of the anhydrous pathway.

On the anhydrous intramolecular proton transfer pathway, the calculated equilibrium reactant and product correspond to the proton adsorbed on O_{b1} and O_t site, respectively, as shown in Figure 5. In the transition state (TS) structure, there is an obvious structural rearrangement of KU cage to facilitate the proton transfer from O_{b1} to O_t. Especially, the W−O_t bond tilts away from its equilibrium position in the octahedron in order to shorten the distance over which the proton is transferred. Simultaneously, the W atom bonded to O_t atom contracts into the KU cage center, leading to a shorter distance between W and P atoms (3.334 Å with respect to normal 3.654 Å).

dx.doi.org/10.1021/ja411268q | J. Am. Chem. Soc. 2014, 136, 4954−4964

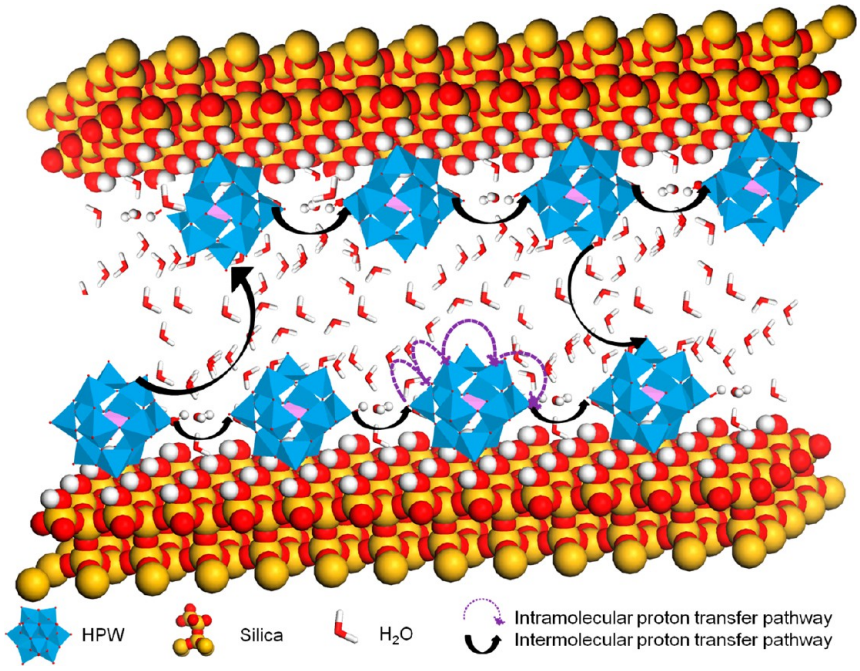

Figure 4. The proton transportation was proposed to occur effectively in two ways. One is the proton-hopping on an isolated phosphotungstic acid, briefly as intramolecular proton transfer pathway. The other is intermolecular proton transfer pathway, in which the proton-exchange process is composed of a series of "hops" among HPW molecules and water molecules along the hydrogen bond.

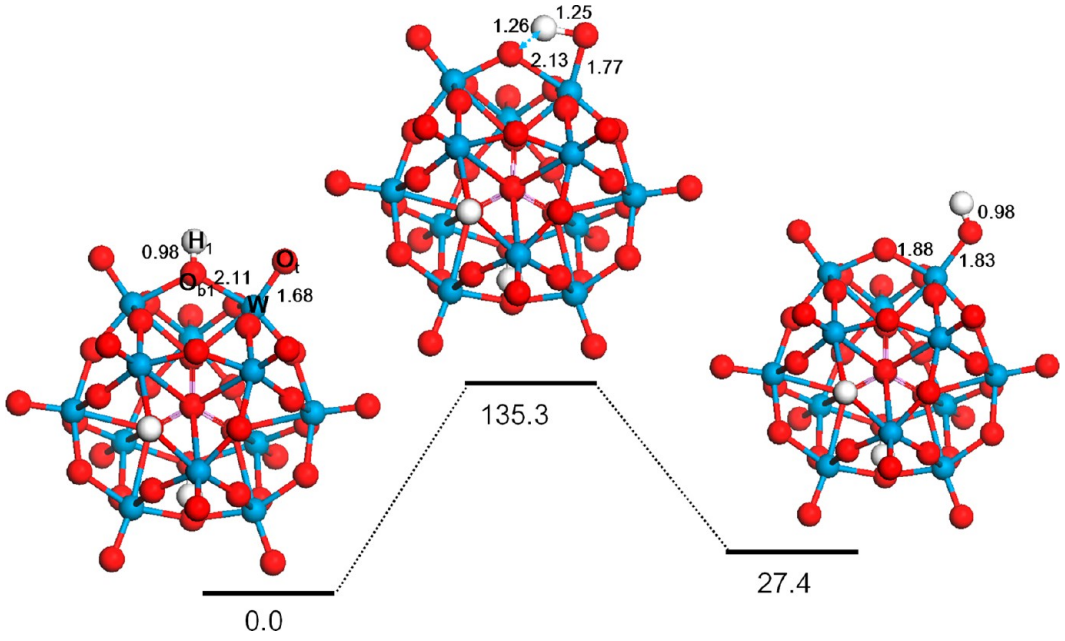

Figure 5. The calculated structure of initial, final, and transition states for the anhydrous proton-hopping reaction between an O_{b1} atom and an O_t atom of HPW. Selected bond lengths are provided in each structure (Å); refer to Table 1 for details. (energy in kJ mol^{-1}).

Additionally, the angle of $\angle O_{b1}-W-O_t$ greatly decreasing to promote the movement of proton along a hydrogen bond between the O_{b1} and O_t atoms. However, the hydrogen-bonding interaction is not effective enough because the $\angle O_{b1}-H-O_t$ angle is 133.4°, far from the ideal 180° for proton transfer in water networks. The energy barrier for transporting proton from O_{b1} site to O_t site is 135.3 kJ mol^{-1}, which is in very good agreement with the previous theoretical result of Janik et al.[16] The detailed structural parameters are listed in Table 1. This high activation energy arises from the substantial structural rearrangements of the transition state for the elementary proton-hopping step.

With the adsorption of one water molecule, the relative orientation of water approaching different acidic protons leads to three different equilibrium structures. Figure 6a shows the initial and final structures for a water molecule bonding to the exterior O_{b1} and O_t of KU with one hydrogen atom of water directing toward the nearest O_t and O_{b1}, respectively. Here the TS involves a six-membered ring structure with two hydrogen bonds, in which the water molecule withdraws a third proton to form a separated hydronium ion H_3O^+ with interactions to O_{b1}

dx.doi.org/10.1021/ja411268q | J. Am. Chem. Soc. 2014, 136, 4954−4964

Table 1. The Simulated Interatomic Distances and Angles of the Initial State, Transition State (TS), and Final State for Intramolecular Proton Transferring from O_{b1} to O_t on Anhydrous, One-, and Two-Water-Assisted Pathways (Angle in Degrees, Distance in Å)[a]

	anhydrous			1 H_2O-assisted			2 H_2O-assisted		
	initial	TS	final	initial	TS	final	initial	TS1	final
$\angle O_{b1}-W-O_t$	94.5 (94.0)	72.1 (71.1)	98.3 (98.0)	94.2	91.4	95.0	96.3	95.2	94.7
$\angle H-O_{b1}-W-O_t$	19.6 (17.1)	1.0 (0.6)	1.6 (0.3)	16.1	5.9	2.77	166.5	147.0	147.7
$\angle O_{b1}-H_1-O_W$				171.0 (162.9)	152.1 (151.9)	125.2 (137.5)	178.6	96.9	74.8
$\angle O_t-H_2-O_W$				119.9 (140.1)	153.9 (156.4)	168.9 (162.8)	94.4	135.3	170.0
$O_{b1}-H_1$	0.99 (0.98)	1.26 (1.26)	2.89 (2.94)	1.04 (1.05)	1.56 (1.56)	2.36 (1.92)	1.28	2.58	3.07
O_W-H_1				1.52 (1.47)	1.05 (1.04)	0.98 (0.99)	1.15	0.98	0.98
O_W-H_2				0.98 (0.99)	1.08 (1.11)	1.45 (1.44)	0.98	0.99	1.04
O_t-H_2	2.80 (2.80)	1.25 (1.25)	0.98 (0.98)	2.50 (1.89)	1.44 (1.37)	1.06 (1.07)	3.15	1.96	1.57
O_W-H_3				0.97 (0.97)	0.98 (0.98)	0.97 (0.98)	1.05	1.25	1.13
$O_{b1}-W$	2.11 (2.12)	2.12 (2.17)	1.88 (1.91)	2.07 (2.08)	2.02 (2.02)	1.93 (1.97)	2.01	1.94	1.93
O_t-W	1.68 (1.71)	1.77 (1.80)	1.83 (1.85)	1.69 (1.73)	1.73 (1.77)	1.79 (1.81)	1.68	1.71	1.73
W–P	3.50 (3.54)	3.33 (3.36)	3.42 (3.45)	3.51	3.47	3.44	3.53	3.53	3.51

[a]aData in parentheses are taken from Reference 16.

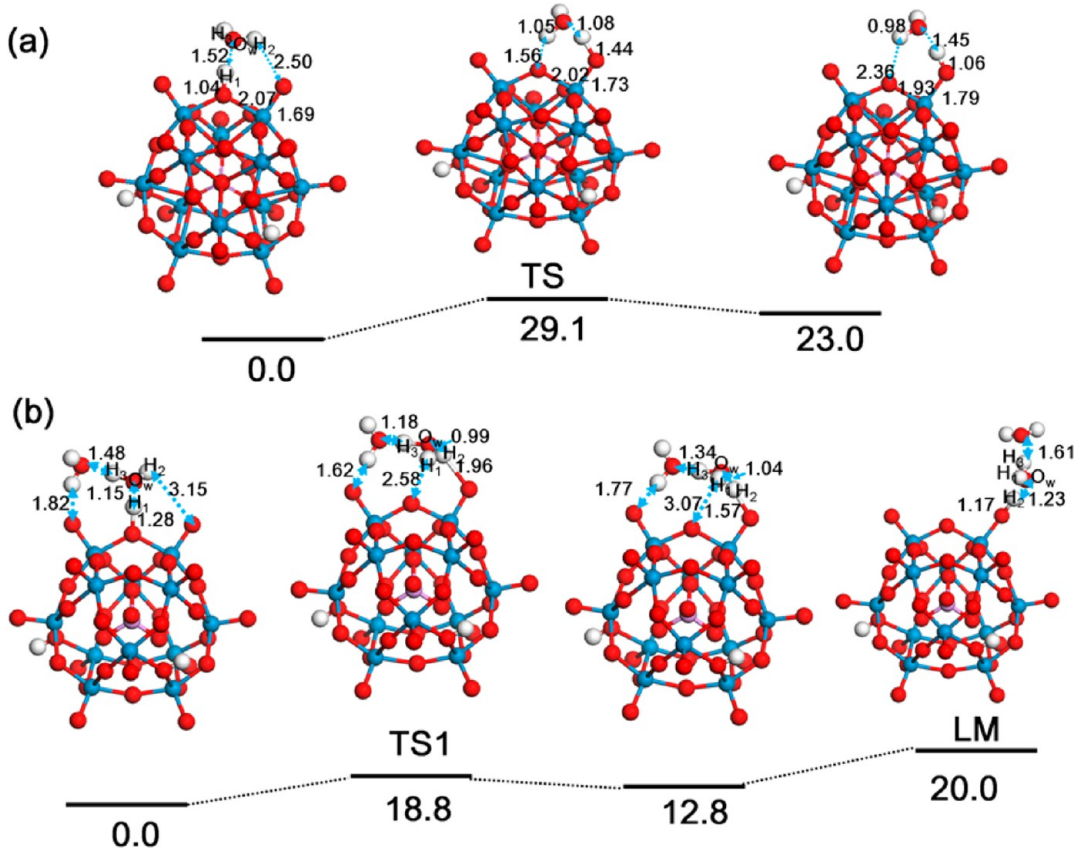

Figure 6. The calculated structure of initial, final, and transition states for the one water-assisted (a) and two water-assisted proton-hopping reactions (b) between an O_{b1} atom and an O_t atom of HPW. Selected bond lengths are provided in each structure (Å); refer to Table 1 for details. (energy in kJ mol^{-1}). TS: transition state; LM: local minimum.

and O_t along the hydrogen bond. Here the two hydrogen-bond angles are 152.1° and 153.9°, respectively. In contrast to the anhydrous pathway, the bonds between the acidic proton and O_{b1}, O_t are both lengthened because of the hydrogen-bonding interaction with water. Furthermore, both the hydrogen-bond angle in initial ($\angle O_{b1}-H_1-O_w$) and final ($\angle O_t-H_2-O_w$) states are much closer to the ideal 180°. Therefore, the proton-hopping reaction path with water assistance is greatly facilitated by the hydrogen-bond interactions since little structural change is needed to facilitate the proton movement. This leads to a much lower potential-energy surface (PES) along the reaction coordinate compared to that of anhydrous proton hopping. Indeed, the calculated activation energy for intramolecular proton transfer assisted with one water decreases to 29.1 kJ mol^{-1}, which is much lower than the energy barrier of anhydrous proton-hopping pathway, and compares favorably with the experimental value of Janik et al.[16]

dx.doi.org/10.1021/ja411268q | J. Am. Chem. Soc. 2014, 136, 4954−4964

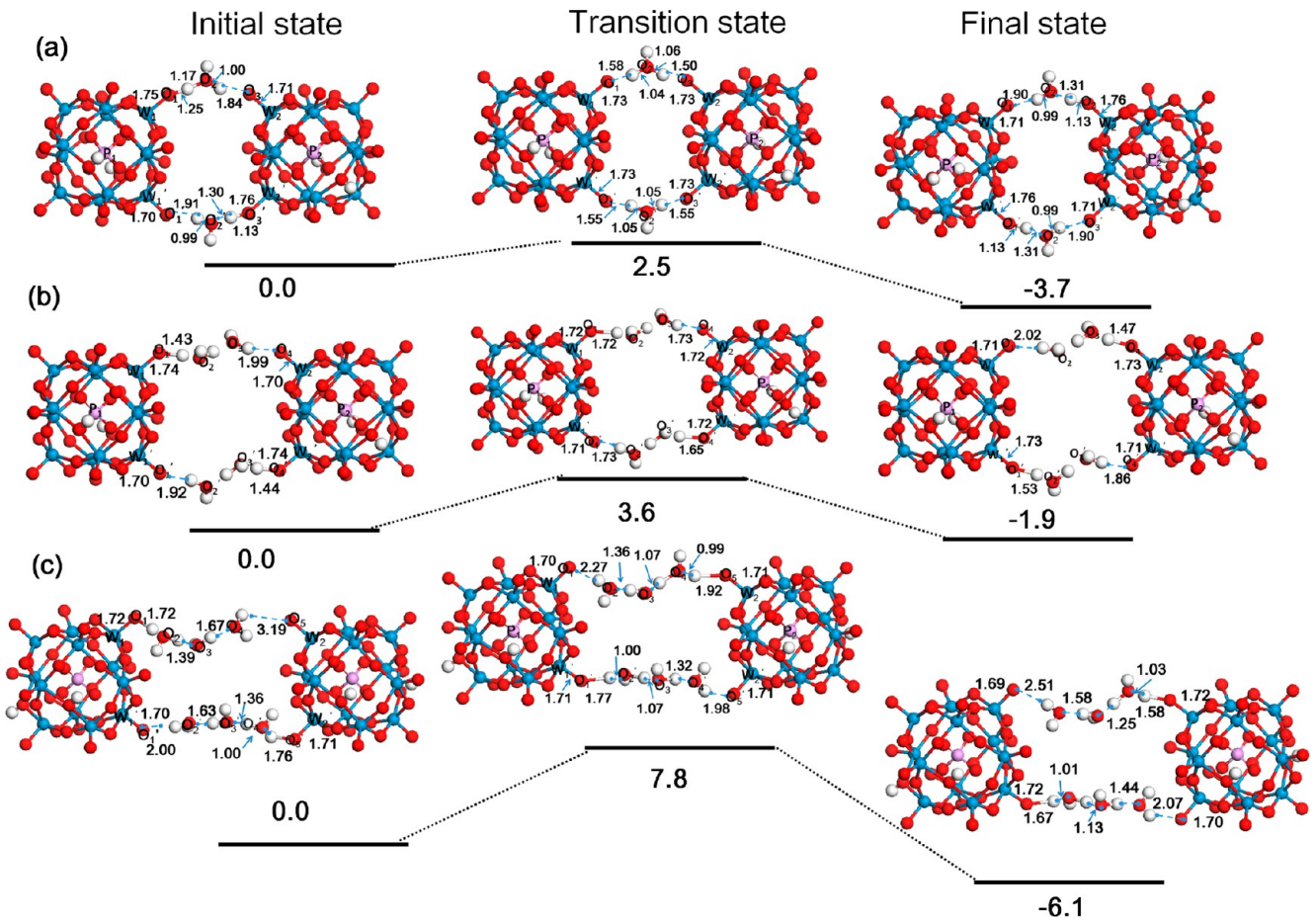

Figure 7. The calculated equilibrium states and transition state for one-water-assisted (a), two-water-assisted (b), and three-water-assisted (c) intermolecular proton-hopping reactions between two HPW molecules (distance in Å, energy in kJ mol^{-1}).

Because of the critical role of water molecule in facilitating proton movement, we considered also the pathway for proton transfer with a second water molecule involved. As depicted in Figure 6b, the optimized initial equilibrium structure involves a new eight-membered ring structure instead of the six-membered ring (Figure 5a) formed when one water is adsorbed at the proton. The second water molecule adsorbs on the adjacent O_t site with a weak hydrogen-bonding interaction (O···H distance at 1.82 Å), in which the oxygen of the water directs toward proton (H_3) of the first water (H_3–O_W–H_2) to form the hydrogen-bonding interaction (O···H distance at 1.48 Å). With the help of the second water, the proton (H_1) gets closer to the O_w atom, which lengthens the distance between O_{b1} and H_1 from 1.04 to 1.28 Å, and shortens bond of O_w–H_1 from 1.52 to 1.15 Å (Table 1). These changes in the structural parameters suggest a weakening of the O_{b1}–H bond strength, which leads to a lower barrier for proton transfer compared with the one-water-assisted pathway. In the optimized TS1, H_1 binds tightly with the O_w atom to form a cation cluster $H_5O_2^+$ that combines with the interaction of the second water molecule. Because of the desorption of H_1 from the O_{b1} site, the two ring structures in the initial equilibrium structure combine into a large 10-membered ring structure in the TS. Subsequently, the proton H_2 attaches on the O_t site to form a new O–H bond. As predicted above, the calculated energy barrier of intramolecular proton hopping pathway decreased further with the assistance of the second water molecule, leading to 18.8 kJ mol^{-1}. This decrease of the energy barrier indicates the dominant role of water in facilitating the proton movement through the hydrogen-bonding interactions. Additionally, we see that the involvement of the second water makes the PES flatter. To break the weak hydrogen interaction between water and terminal oxygen atoms in the final state, an additional energy of 7.2 kJ mol^{-1} is needed to make the $H_5O_2^+$ cluster to desorb from the HPW unit. With the new local minimum (LM) without the extra interaction between $H_5O_2^+$ cluster and HPW, the proton has a lower barrier to reach the adjacent molecular HPW, as will be discussed in detail in the following section.

In the above intramolecular proton transfer pathway, the adsorption of one water molecule substantially reduces the activation barrier of proton-hopping to 29.1 kJ mol^{-1}, while two-water-assisted pathway reduces it further to 18.8 kJ mol^{-1}, since no substantial structural rearrangement of the KU cage is required to facilitate the proton movement in contrast to the anhydrous proton transfer pathway. Especially, the involvement of a second water molecule allows formation of a transition state with a large 10-membered ring, leading the energy barrier of proton transfer reaction to be decreased further. The results of this calculation are in excellent agreement with recent theoretical results that find a small amounts of water greatly enhance the overall rate of proton movement.[16]

4.2. InterHPW Proton Hopping. However, both intramolecular proton transfer pathway and intermolecular proton transfer pathway between adjacent HPWs in PEM must be considered to obtain the overall proton conductivity as

dx.doi.org/10.1021/ja411268q | J. Am. Chem. Soc. 2014, 136, 4954–4964

Table 2. The Simulated Interatomic Distances and Angles of the Reactant, Transition State (TS), and Product Structures for Intermolecular Proton Transfer Pathway with One-, Two-, and Three-Water Assistance via Water-Formed H-Bonding Bridges (Angle in Degrees, Distance in Å)

	1 H_2O-assisted			2 H_2O-assisted			3 H_2O-assisted		
	initial	TS	final	initial	TS	final	initial	TS	final
$\angle W_1-O_1-H$	157.8	154.0	151.9	134.1	134.0	152.0	113.5	135.4	144.4
$\angle W_2-O_3-H$	146.8	151.2	151.9						
$\angle W_2-O_4-H$				143.7	147.1	151.9			
$\angle W_2-O_5-H$							143.1	140.3	152.5
W_1-O_1	1.75	1.73	1.71	1.74	1.72	1.71	1.72	1.70	1.69
O_1-H	1.17	1.58	1.90	1.43	1.72	1.47	1.72	2.27	2.51
$O_1\cdots O_2$	2.42	2.60	2.86	2.51	2.75	3.00	2.73	3.25	3.48
$O_2\cdots O_3$	2.80	2.55	2.44	2.52	2.53	2.52	2.48	2.45	2.61
$O_3\cdots O_4$				2.95	2.75	2.53	2.68	2.49	2.44
$O_4\cdots O_5$							3.63	2.87	2.60
O_3-W_2	1.71	1.73	1.76						
O_4-W_2				1.70	1.72	1.73			
O_5-W_2							1.69	1.71	1.72
$\angle W_2'-O_3'-H$	151.6	152.7	144.9						
$\angle W_2'-O_4'-H$				134.8	135.0	152.0			
$\angle W_2'-O_5'-H$							116.2	118.9	118.9
$W_2'-O_3'$	1.76	1.73	1.73						
$W_2'-O_4'$				1.74	1.72	1.71			
$W_2'-O_5'$							1.71	1.71	1.70
$O_3'-H$	1.13	1.55	1.90						
$O_4'-H$				1.44	1.65	1.53			
$O_5'-H$							1.76	1.98	2.07
$O_5'\cdots O_4'$							2.65	2.84	2.93
$O_4'\cdots O_3'$				2.51	2.68	2.85	2.46	2.44	2.50
$O_3'\cdots O_2'$	2.43	2.58	2.86	2.51	2.50	2.48	2.64	2.50	2.46
$O_2'\cdots O_1'$	2.87	2.58	2.44	2.91	2.75	2.58	2.92	2.76	2.68
$O_1'-W_1'$	1.70	1.73	1.76	1.70	1.71	1.73	1.70	1.71	1.72

indicated from Figure 4. In this section, we report a series of DFT computations to describe the proton movement between the nearest HPW molecules and to estimate the dependence of the activation energy for intermolecular proton-hopping, on the distance of the adjacent HPW molecules.

As shown in Figure 4, the ideal model is too large to treat the entire HPW-*meso*-silica materials into an ab initio manner. However we cannot trust empirical or semiempirical methods, since they may not be sufficiently accurate in describing the weak hydrogen-bond interactions between HPW and water. In order to balance the computational cost and sufficient precision, we constructed an appropriate model as follows. We assume that the distributions of HPW on silica surface are ideally uniform, and used various 2D/3D models to estimate the average distance between two nearest HPW molecules based on the weight percentage (for details see Supporting Information). Since we expect strong binding of HPW molecules to the silica surface we anticipate little change in the distance between the neighboring HPW during the process of proton transport. Considering that the effective screening of the system results in negligible additional electrostatic interaction between the adjacent HPW units in the course of proton transfer process, we keep each of HPW molecule neutral by either donating a proton or removing a proton for the clusters. Herein, we propose that when one HPW gives one proton to the neighboring one (top reaction pathway), it will simultaneously receive a proton from other HPW (bottom reaction pathway), Thus both donors and acceptors are involved in the proton-transfer reactions as depicted in Figure 7. With these theoretical considerations and assumptions, we build a simplified model composed of two neutral KU phosphotungstic acid molecules with fixed distance, which were subjected to a full electron treatment as described in in the Computational Methods section.

Figure 7a shows the optimized structures with one-water-assisted intermolecular proton transfer pathway, in which the two neutral KU HPW molecules fixed at 12.6 Å (central P···P distance). And two water molecules are in the middle of the two HPW units, which interact with the acidic proton of HPW through hydrogen bond. Similar to the intramolecular proton transfer pathway, the water molecule adsorbs on the acidic proton. Simultaneously, it interacts weakly with another exterior oxygen atom (O_3) in the neighboring HPW molecule through hydrogen-bonding interaction.

In the initial site for the one-water promoted intermolecular proton transfer, the bonds between the acidic protons and the O_t atoms (O_1 and O_3') lengthen slightly with respect to the intramolecular water-assisted proton transfer pathway, which may result from the ideal 180° angles ($\angle O_1-H-O_2$ and $\angle O_3'-H-O_2'$) for efficient proton transfer pathway. Considering the transition state shown in Figure 7a, the water molecule also appears as a separated hydronium ion H_3O^+, which interacts with both O_t (O_1 and O_3, O_1' and O_3') of neighboring HPW molecules. The intermolecular one-water-assisted proton transfer from O_1 to O_3, together with O_3' to O_1', occurs by the movement of protons along the two hydrogen-bond directions. Despite this complexity, Figure 7a and Table 2 clearly indicate that there is little structural

dx.doi.org/10.1021/ja411268q | J. Am. Chem. Soc. 2014, 136, 4954−4964

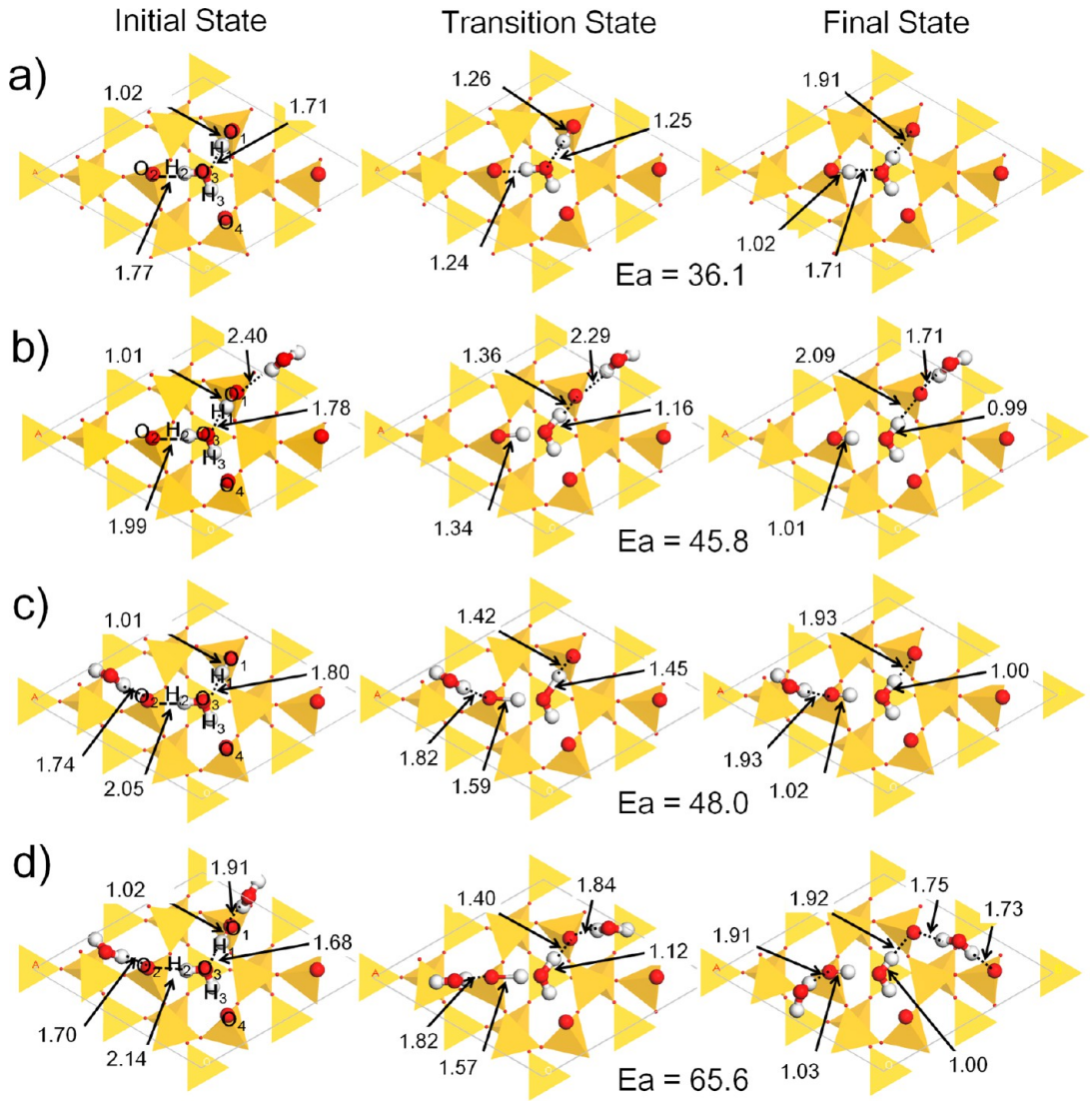

Figure 8. The calculated equilibrium states and transition states for water-assisted proton-hopping reactions on $SiO_2(111)$ surface with different coverage of water. The estimated activation energy for movement of proton on $SiO_2(111)$ is 36.1 (a), 45.8 (b), 48.0 (c), and 65.6 kJ mol^{-1} (d), respectively (distance in Å).

arrangement in the process. The result is an activation barrier for the intermolecular proton transfer process of only 2.5 kJ mol^{-1}, which is much lower than the barrier of the water-assisted intramolecular proton transfer pathways.

On the basis of the TEM results, we conclude that as the concentration of HPW decreases in HPW-*meso*-silica PEM, the average distance between the neighboring HPW molecules must increase accordingly. Consequently we studied the energetics associated with proton-hopping between HPW at distances of 15.0 and 17.0 Å to estimate the effect of the content of HPW on the proton conductivity observed in experiments (Figure 2). This provides deep insight into the mechanism of proton movement within HPW-*meso*-silica PEM.

With the distance between two central P atoms at 15.0 Å, we find two water molecules to form hydrogen bonds with acidic protons as shown in Figure 7b in both the up and bottom pathways. Similar to the results of one-water-assisted intermolecular proton movement in Figure 7a, the water molecules directly linked the two O_t atoms (O_1 and O_4', O_1' and O_4) of molecular HPW. In the initial structure, the two acidic protons adsorbed on O_1 and O_4' with O−H bond length of 1.43 and 1.44 Å, respectively, which are slightly higher than that in one-water-assisted reactant. In the final site, the two protons were linked to O_4 and O_1', respectively. The equilibrium and transition states for two-water-assisted intermolecular proton-exchange reactions are illustrated in Figure 7b, with the interatomic distances and angles given in Table 2. We see that the motions of proton between the nearest KUs are composed of a series of "hops", which include the transferring of proton from residing on O_t (O_1 and O_4') of the KU to the nearest water molecules, migrating within $H_5O_2^+$ clusters formed via hydrogen-bonding interactions, sticking again to another O_t site (O_4 and O_1') of KU finally. The estimated activation energy for this series of proton hops is 3.8 kJ mol^{-1}, slightly higher than that of one-water-assisted intermolecular proton-hopping reaction. This likely stems from the additional bond-forming and breaking associated with the two-water-assisted intermolecular proton-hopping pathway.

When the distance between the nearest phosphotungstic acid molecules was increased further to 17.0 Å, three water molecules were needed to form efficient hydrogen-bonding

dx.doi.org/10.1021/ja411268q | J. Am. Chem. Soc. 2014, 136, 4954−4964

Table 3. The Simulated Interatomic Distances and Angles of the Initial State, Transition State (TS), and Final State for Proton Transferring from O_1 to O_2 on SiO_2(111) Surface Using 2 × 2 Unit Cell (Angle in Degrees, Distance in Å)

	1 H_2O (a)			2 H_2O (b)			2 H_2O (c)			3 H_2O (d)		
	initial	TS	final	initial	TS	final	initial	TS	final	initial	TS	final
$O_1\cdots H_1$	1.02	1.26	1.91	1.01	1.36	2.09	1.01	1.42	1.93	1.02	1.40	1.92
$H_1\cdots O_3$	1.71	1.25	1.00	1.78	1.16	0.99	1.80	1.45	1.00	1.68	1.12	1.00
$O_3\cdots H_2$	1.01	1.27	1.71	1.00	1.17	1.79	1.00	1.31	1.71	0.99	1.06	1.66
$H_2\cdots O_2$	1.77	1.24	1.02	1.99	1.34	1.01	2.05	1.59	1.02	2.14	1.57	1.03
$O_1\cdots H$				2.40	2.29	1.71				1.91	1.84	1.75
$O_2\cdots H$							1.74	1.82	1.93	1.70	1.82	1.91
$O_3\cdots H_3$	1.01	0.99	1.01	1.01	1.01	1.01	1.01	1.01	1.01	1.01	1.00	1.01
$H_3\cdots O_4$	1.78	1.86	1.77	1.78	1.89	1.76	1.80	1.81	1.82	1.77	1.83	1.74
$\angle O_1\cdots H_1\cdots O_3$	168.4	170.5	164.9	164.0	172.2	158.8	163.7	160.9	162.0	171.8	174.7	163.8
$\angle H_1\cdots O_3\cdots H_2$	123.1	127.4	121.7	125.8	132.0	126.6	124.2	124.4	123.7	122.2	124.7	123.1
$\angle O_3\cdots H_2\cdots O_2$	135.4	171.2	171.5	163.5	173.9	164.4	161.5	164.1	169.9	161.0	175.7	172.8
$\angle H_1\cdots O_3\cdots H_3$	118.2	111.4	106.5	119.7	108.9	106.6	120.5	115.1	106.8	120.8	111.9	106.5
$\angle O_3\cdots H_3\cdots O_4$	171.3	169.6	172.9	171.8	171.2	173.4	170.6	172.0	173.4	172.1	172.2	173.5
$\angle H_2\cdots O_3\cdots H_3$	107.0	109.8	117.2	106.5	108.7	122.0	107.4	114.3	121.3	107.6	110.4	119.0

interactions to promote proton-exchange (Figure 7c). The calculated barrier here is 8.0 kJ mol^{-1}, which is substantially higher than for both the one- and two-water-assisted intermolecular proton transfer pathways. This indicates why the activation barrier for proton transfer increases gradually as the distance between HPWs is increased, i.e., as the wt % of HPW decreases. However, we note that all of the activation barriers for intermolecular pathways discussed above are lower than intramolecular proton transfer pathways. This indicated that the overall activation barrier for proton transfer within HPW-*meso*-silica PEM still dominates the intramolecular proton transfer process as the distance between neighboring HPW changes from 12.6 to 17.0 Å.

Adjacent distance between the HPW molecules at 12.6, 15.0, and 17.0 Å are all observed experimentally in the HPW-*meso*-silica PEM with high weight percentage of HPW. Our theoretical investigations confirm that the apparent energy barrier for proton transfer is dominated by the intramolecular proton transfer pathway, which explains well that the barrier deduced from experiment is nearly constant when the wt % of HPW is above 67%. Consequently, it is reasonable to expect that the energy barrier for intermolecular proton-hopping reaction would increase continuously as the distance between the neighboring molecular HPWs increases, going much higher than that of water-insisted intramolecular proton transfer pathway for extremely long distances between HPWs. Herein, the apparent activation barrier should be decided by the intermolecular proton transfer pathway. Therefore, the activation barrier is increased slightly as the wt % of HPW in the range of 10 to 60%, which agrees fairly well with those conclusions in experiment.

4.3. Proton Movement on Pure SiO_2(111) Surface. In experiments, the proton conductivity was very low on *meso*-silica channels with no HPW adsorbed (0% HPW), indicating a high proton transfer activation energy of 46.0 kJ mol^{-1}. In order to delineate the proton movement within *meso*-silica, we chose the most stable surface of silica, the ideal (111) surface of β cristobalite, and calculate the activation energy using 2 × 2 and 3 × 3 units to check the effect of coverage, as well as the concentration of the adsorbed water. These studies part were carried out at a low-level quality for qualitative purposes since for the real materials the geometrical structure of silica surface is too complex to be modeled with a simple model.

In Figure 8, the equilibrium and transition state structures for proton transferring from O_1 to O_2 in 2 × 2 unit cell are shown, together with the structural information in Table 3. Figure 8a shows that for one additional water the proton H_1 binds directly to O_1 with O−H distance of 1.017 Å in the initial structure. And the water molecule adsorbed on the surface with O_3 atom interacting to H_1, H_2, and H_3 weakly bonding toward O_2 and O_4, respectively. In the transition state, the bond, H_1−O_1 is broken, which facilitates bond-forming between H_2 and O_2. Finally, the proton H_2 on silica surface binds to O_2 with distance of 1.108 Å. The activation energy for proton-hopping from O_1 to O_2 is 36.1 kJ mol^{-1}, which is much higher than the water-assisted inter/intramolecular proton movement. Increasing the size of the periodic supercell to 3 × 3 (Supporting Information), the calculated activation energy for proton movement increased to 51.5 kJ mol^{-1} which indicates that the barrier for proton hopping in silica surface without HPW adsorbed is too high for proton transport.

Considering the effect from the concentration of water molecule, we studied the two- and three-water-assisted proton transfer pathways on silica surface. In Figure 8b,c, the second water molecules adsorb on surface through weak interactions toward O_1 and O_2, respectively. In contrast to the intramolecular proton-hopping process, the energy barriers do not decrease slightly, but rather they increase up to 45.8 and 48.0 kJ mol^{-1} in the two-water-assisted pathway, which are very close to the higher barrier measured in experiment (Figure 2b). Indeed the barrier of the proton transfer reaction is even higher of 65.6 kJ mol^{-1} when three water molecules approach to the silica surface. Therefore, the proton conductivity is quite low because of the high barrier for proton movement on pure silica in any coverage of water.

5. CONCLUSIONS

In summary, the experimental studies show that the proton conductivity and the activation energy for proton transport within the HPW-*meso*-silica membrane is highly dependent on the HPW content. Our mechanism of proton transfer within HPW-based proton-exchange membrane derived from the DFT calculations explains the strong dependence of the conductivity and activation barrier on the concentration of HPW. At very high concentration of HPW (67−83 wt %), the distance between the neighboring HPWs is less than 17.0 Å. The

dx.doi.org/10.1021/ja411268q | J. Am. Chem. Soc. 2014, 136, 4954−4964

corresponding activation energy of intermolecular proton transfer is much lower than the water-assisted intramolecular proton transfer pathway. Therefore, the activation barrier of intramolecular proton transfer is the rate-determining step. On the clean silica surface without adsorbed HPW, the activation barrier is too high for proton transport. The present investigations provide an improved understanding of the proton transport mechanism within proton-exchange membrane, and useful guidance in designing new inorganic-material-based proton-exchange membrane.

■ ASSOCIATED CONTENT

Supporting Information

The calculated proton affinity (eV) and R_{P-H} distance (pm) for the $[PW_{12}O_{40}]^{3-}$ anion, distance between two nearest HPW molecules, interatomic distances and angles of the reactant (R_1), transition state (TS) and product (P_1) structures for proton transferring from O_{b1} to O_t on anhydrous HPW; the scheme and structural details of three-water-assisted proton-hopping process between two phosphotungstic acid molecules; the scheme and structural details of water-assisted proton-hopping reactions on $SiO_2(111)$ surface. This material is available free of charge via the Internet at http://pubs.acs.org.

■ AUTHOR INFORMATION

Corresponding Author

hbsu@ntu.edu.sg; s.jiang@curtin.edu.au; wag@wag.caltech.edu

Notes

The authors declare no competing financial interest.

■ ACKNOWLEDGMENTS

The project was supported by the AcRF Tier 2 of Ministry of Education, Singapore (T208A1216); A*STAR SERC Grant, Singapore (1121202012); National Research Foundation, Singapore; the Australian Research Council (ARC DP120102325) and US NSF (CBET-1067848).

■ REFERENCES

(1) Jacobson, M. Z.; Colella, W. G.; Golden, D. M. *Science* **2005**, *308*, 1901.

(2) Nogami, M.; Matsushita, H.; Goto, Y.; Kasuga, T. *Adv. Mater.* **2000**, *12*, 1370.

(3) Agnolucci, P. *Int. J. Hydrogen Energy* **2007**, *32*, 4306.

(4) Costamagna, P.; Srinivasan, S. *J. Power Sources* **2001**, *102*, 253.

(5) Jiang, S. P.; Liu, Z. C.; Tian, Z. Q. *Adv. Mater.* **2006**, *18*, 1068.

(6) (a) Alberti, G.; Casciola, M.; Palombari, R. *J. Membr. Sci.* **2000**, *172*, 233. (b) Herring, A. M. *Polym. Rev.* **2006**, *46*, 245.

(7) (a) Malhotra, S.; Datta, R. *J. Electrochem. Soc.* **1997**, *144*, L23. (b) Ramani, V.; Kunz, H. R.; Fenton, J. M. *J. Power Sources* **2005**, *266*, 110. (c) Ramani, V.; Kunz, H. R.; Fenton, J. M. *Electrochim. Acta* **2005**, *50*, 1181.

(8) (a) Li, H. B.; Nogami, M. *Adv. Mater.* **2002**, *14*, 912. (b) Athens, G. L.; Ein-Eli, Y.; Chmelka, B. F. *Adv. Mater.* **2007**, *19*, 2580. (c) Colomer, M. T. *Adv. Mater.* **2006**, *18*, 371. (d) Yamada, M. D.; Li, L.; Honma, I.; Zhou, H. S. *J. Am. Chem. Soc.* **2005**, *127*, 13092. (e) Daiko, Y.; Kasuga, T.; Nogami, M. *Chem. Mater.* **2002**, *14*, 4624. (f) Li, H. B.; Nogami, M. *Chem. Commun.* **2003**, 236. (g) Xiong, L. M.; Nogami, M. *Chem. Lett.* **2006**, *35*, 972. (h) Vichi, F. M.; Tejedor-Tejedor, M. I.; Anderson, M. A. *Chem. Mater.* **2000**, *12*, 1762.

(9) Marschall, R.; Sharifi, M.; Wark, M. *Microporous Mesoporous Mater.* **2009**, *123*, 21.

(10) Halla, J. D.; Mamak, M.; Williams, D. E.; Ozin, G. A. *Adv. Funct. Mater.* **2003**, *13*, 133.

(11) (a) Uma, T.; Nogami, M. *J. Membr. Sci.* **2009**, *334*, 123. (b) Uma, T.; Nogami, M. *J. Membr. Sci.* **2008**, *323*, 11. (c) Inoue, T.; Uma, T.; Nogami, M. *J. Membr. Sci.* **2008**, *323*, 148. (d) Uma, T.; Nogami, M. *Fuel Cells* **2007**, *7*, 279. (e) Uma, T.; Nogami, M. *J. Electrochem. Soc.* **2007**, *154*, B845.

(12) Uma, T.; Nogami, M. *Anal. Chem.* **2008**, *80*, 506.

(13) Uma, T.; Nogami, M. *Chem. Mater.* **2007**, *19*, 3604.

(14) (a) Lu, S. F.; Wang, D. L.; Jiang, S. P.; Xiang, Y.; Lu, J. L.; Zeng, J. *Adv. Mater.* **2010**, *22*, 971. (b) Zeng, J.; Jiang, S. P. *J. Phys. Chem. C* **2011**, *115*, 11854. (c) Zeng, J.; Shen, P. K.; Lu, S. F.; Xinag, Y.; Li, L.; De Marco, R.; Jiang, S. P. *J. Membr. Sci.* **2012**, *397*−*398*, 92. (d) Zeng, J.; Jin, B. Q.; Shen, P. K.; He, B. B.; Lamb, K.; De Marco, R.; Jiang, S. P. *Int. J. Hydrogen Energy* **2013**, *12830*−*12839*, 38.

(15) (a) Tang, H. L.; Pan, M.; Lu, S. F.; Lu, J. L.; Jiang, S. P. *Chem. Commun.* **2010**, *46*, 4351. (b) Tang, H. L.; Pan, M.; Jiang, S. P. *Dalton Trans.* **2011**, *40*, 5220. (c) Lu, J. L.; Tang, H. L.; Lu, S. F.; Wu, H. W.; Jiang, S. P. *J. Mater. Chem.* **2011**, *21*, 6668.

(16) Janik, M. J.; Davis, R. J.; Neurock, M. *J. Am. Chem. Soc.* **2005**, *127*, 5238.

(17) (a) Li, Z.; Chen, D. H.; Tu, B.; Zhao, D. Y. *Microporous Mesoporous Mater.* **2007**, *105*, 34. (b) Chen, D.; Li, Z.; Yu, C.; Shi, Y.; Zhang, Z.; Tu, B.; Zhao, D. *Chem. Mater.* **2005**, *17*, 3228.

(18) Zeng, J.; Zhou, Y. H.; Li, L.; Jiang, S. P. *Phys. Chem. Chem. Phys.* **2011**, *13*, 10249.

(19) Kozhevnikov, I. V.; Sinnema, A.; Jansen, R. J.; Vanbekkum, H. *Catal. Lett.* **1994**, *27*, 187.

(20) Lefebvre, F. *J. Chem. Soc., Chem. Commun.* **1992**, 756.

(21) Nakamura, O.; Kodama, T.; Ogino, I. *Chem. Lett.* **1979**, 17.

(22) (a) Delley, B. *J. Chem. Phys.* **1990**, *92*, 508. (b) Delley, B. *J. Chem. Phys.* **2000**, *113*, 7756. Dmol3 is available as part of Material Studio.

(23) Perdew, J. P.; Burke, K.; Ernzerhof, M. *Phys. Rev. Lett.* **1996**, *77*, 3865.

(24) (a) Dolg, M.; Wedig, U.; Stoll, H.; Preuss, H. *J. Chem. Phys.* **1987**, *86*, 866−872. (b) Bergner, A.; Dolg, M.; Küchle, W.; Stoll, H.; Preuss, H. *Mol. Phys.* **1993**, *80*, 1431−1441.

(25) Ceresoli, D.; Bernasconi, M.; Iarlori, S.; Parrinello, M.; Tosatti, E. *Phys. Rev. Lett.* **2000**, *84*, 3887.

(26) Halgren, T. A.; Lipscomb, W. N. *Chem. Phys. Lett.* **1977**, *49*, 225.

(27) (a) Kozhevnikov, I. V. *Russ. Chem. Rev.* **1987**, *56*, 811. (b) Okuhara, T.; Mizuno, N.; Misono, M. *Adv. Catal.* **1996**, *41*, 113. (c) Bardin, B. B.; Bordawekar, S. V.; Neurock, M.; Davis, R. J. *J. Phys. Chem. B* **1998**, *102*, 10817.

(28) (a) Dec, S. F.; Herring, A. M. *J. Phys. Chem. B* **2004**, *108*, 12339. (b) Slade, R. C. T.; Omana, M. J. *Solid State Ionics* **1992**, *58*, 195. (c) Slade, R. C. T.; Pressman, H. A.; Skou, E. *Solid State Ionics* **1990**, *38*, 207. (d) Pressman, H. A.; Slade, R. C. T. *Chem. Phys. Lett.* **1988**, *151*, 354. (e) Kreuer, K. D.; Hampele, M.; Dolde, K.; Rabenau, A. *Solid State Ionics* **1988**, *28*, 589. (f) Hardwick, A.; Dickens, P. G.; Slade, R. C. T. *Solid State Ionics* **1984**, *13*, 345.

(29) Pettersson, A.; Rosenholm, J. B. *Langmuir* **2002**, *18*, 8447.